Generalized Moment Description of Brownian Dynamics in Biological Systems

K. Schulten, A. Brünger, W. Nadler, and Z. Schulten

Physik Department, Technische Universität München
D-8046 Garching, Fed. Rep. of Germany

1. Introduction

Many biological processes are controlled by the time that the participating biomolecules need to diffuse around and encounter each other. Nature has devised, therefore, a variety of ways to shorten this time by guiding biomolecules into lower dimensional spaces, e.g., into the plane of membranes. Still the time spent on Brownian motion before the actual molecular reactions is exceedingly long compared to the time scale of the single diffusive displacements. Brownian transport processes also play a role in elementary biological reactions lasting as short as 10^{-12}s since even on this time scale the motion of molecules and molecular fragments in the dense biological media at physiological temperatures is of a Brownian nature. One may envisage that in such situations the fastest Brownian relaxation processes govern the reaction dynamics. This is not the case as is shown by a typical biochemical reaction proceeding along a reaction coordinate with a potential barrier. Diffusive barrier crossing is a very slow process and occurs only in the long time tail of Brownian relaxation. In recent years it has become apparent that proteins, the main carriers of biological function, exhibit an intrinsic dynamic disorder. The disorder originates from a local Brownian motion of the constituent atoms[1]. Fluctuations of the protein conformations which contribute to the protein function again occur very slowly compared to the time scale of local Brownian motion. All the processes described which last as long as 1 min and as short as 10^{-12}s require a description which accounts properly for the long time behavior of the intrinsic stochastic dynamics. In this article we will provide such a mathematical description. The mathematical derivation is based on 2-sided Padé approximants which reproduce the long-time behavior as well as the short-time behavior, i.e., the initial state. The description is applied to three sample situations: linear diffusive transport, lateral diffusion in membranes, and protein dynamics.

2. Observables

In this Section we define formally a class of observables which allow the monitoring of stochastic processes as they occur in biological systems. In the following section we will provide examples of such observables.

A particle under the influence of a potential $U(x)$ and a random force $F(t)$ and friction γ is described by the Langevin equation (for the general theory see Ref. 2,3)

$$m\ddot{x} = -\partial_x U(x) - \gamma\dot{x} + F(t) \quad . \tag{1}$$

In the case of white noise and strong friction conditions which apply in condensed biological media at physiological temperatures, after times of about 10^{-12}s the distribution $p(x,t|x_0)$ for an ensemble of biological particles initially (t = 0) at position x_0 satisfies the Fokker-Planck equation ($\beta = 1/kT$)

$$\partial_t p(x,t|x_0) = L(x)p(x,t|x_0) \tag{2}$$

$$p(x, t=0 | x_o) = \delta(x - x_o) \tag{2b}$$

$$L(x) = \partial_x D(x)\{\partial_x + \beta[\partial_x U(x)]\} - k(x) . \tag{2c}$$

These equations have to be complemented by two spatial boundary conditions at $x = x_i$, $i = 1,2$

$$D(x)\{\partial_x + \beta[\partial_x U(x)]\}p(x,t|x_o) = \kappa_i \, p(x,t|x_o) \tag{2d}$$

in case the diffusion space is confined to the interval $[x_1, x_2]$.[4]

In Eq.(2c) the first term describes the diffusive displacements of particles, the second term the drift in the force field $-\partial_x U(x)$, and the last term the occurrence of a possible first-order reaction with a rate constant $k(x)$. The Fokker-Planck equation (2) assumes a one-dimensional stochastic motion. The following theory is not restricted to this dimensionality.

We will consider the following class of observations: Particles are initially prepared in a distribution $v(x_o)$, most commonly a Boltzmann distribution. The particles propagate then according to Eq.(2) and are observed at time t at position x with a weight $w(x)$. The resulting observable is

$$J(t) = \int dx \int dx_o \, w(x) \, p(x,t|x_o)v(x_o) . \tag{3}$$

This can also be expressed in terms of the Fokker-Planck operator $L(x)$. It is actually most convenient to consider in the following the Laplace transform of (3) expressed by $L(x)$

$$\hat{J}(\omega) = \int dx \, w(x)\{[\omega - L(x)]^{-1}\}_b \, v(x) . \tag{4}$$

Here $\{....\}_b$ denotes that the operator $....$ is restricted to a function space in which all functions obey (2d).

In some instances an expression in terms of the adjoint Fokker-Planck operator $L^+(x)$

$$L^+(x) = \partial_x D(x)\partial_x - \beta[\partial_x U(x)]\partial_x - k(x) \tag{5}$$

may be preferred

$$\hat{J}(\omega) = \int dx \, v(x)\{[\omega - L^+(x)]^{-1}\}_{b^+} \, w(x) . \tag{6}$$

In this expression $\{...\}_{b^+}$ denotes that the function space is restricted to functions which obey the boundary condition adjoint to (2d)

$$D(x)\partial_x \, p(x,t|x_o) = \kappa_i \, p(x,t|x_o) \tag{7}$$

The derivation of this condition involves a generalization of Green's theorem and the requirement that the concomitant of $L(x)$ and $L^+(x)$ vanishes on the boundary.

Equations (4) and (6) provide the most concise representation of the observables of interest and will be employed to construct proper approximations. $\hat{J}(\omega)$ as given by (4) and (6) are commonly referred to as correlation functions.

3. Examples

In our first example of observables of the type (4) or (6) we consider particles which diffuse freely $[U(x)\equiv 0]$ in the interval $[x_1, x_2]$. The diffusion is a prototype transport process which occurs intermediately between biochemical reactions. Of interest is the time which a biomolecule needs to arrive at its target. In our example the particles are initially positioned at $x = x_1$ and become absorbed if they

reach the target positioned at $x = x_2$. The process is characterized by $L(x) = D\partial_x^2$ and by boundary conditions with $\kappa_1 = 0$ and $\kappa_2 \to \infty$. The latter corresponds to

$$p(x,t \mid x_o) = 0 \qquad \text{at } x = x_2 \quad . \qquad (8)$$

The observable of interest is the rate $r(t)$ of absorption by the target and can be expressed as the time derivative of the number of particles $N(t \mid x_o)$ not absorbed yet at time t. $N(t \mid x_o)$ is of the type (4) with $v(x) = \delta(x-x_o)$ and $w(x) \equiv 1$. The rate can be evaluated exactly by means of a spectral expansion .

$$r(t) = \sum_{n=0}^{\infty} (-1)^n [(2n+1)\pi D/a^2] \exp[-(2n+1)^2 \pi^2 Dt/4a^2] . \qquad (9)$$

This result furnishes a test of the approximation developed in Section 4. It should be pointed out, however, that the approximation to be developed can deal with more general situations than those considered in this example. For example, it can deal with a diffusion process with potential barriers lying between the initial position x_1 and the target position x_2.

The second example concerns an experimental method to measure the lateral diffusion in biological membranes, the "continuous fluorescence microphotolysis" method[5]. In an observation a laser beam with profile $k(r)$ is focused through a microscope to irradiate a small spot on a biological membrane with diameter of about 1μm. The membrane constituents that one wishes to study, i.e., proteins or lipids, are labeled with dye molecules which are partially damaged by the irradiation. The undamaged dyes fluoresce the incident light. The fluorescence is observed and provides information on the mobility of the dye-labeled membrane constituents. If one assumes a rotationally symmetric laser profile $k(r)$, the relevant radial Fokker-Planck operator for the distribution of the dye-labeled molecules is for flat membranes

$$L(r) = (D/r)\partial_r r \partial_r - k(r) \qquad (10)$$

where the second term accounts for the photoreaction (damage) of the dyes, a process which is assumed to be first order. The observed fluorescence intensity is then described by an observable as given by Eq.(4) with $v(r) = 1$. Since the fluorescence of the dyes is proportional to the laser intensity, the weight function is given by the laser profile, i.e., $w(r) = k(r)$, except for an overall unimportant factor. The observable can be written

$$\hat{J}(\omega) = \int d^2r \, k(r)\{[\omega - L(r)]^{-1}\}_b \, 1 \quad .$$

The third example concerns the dynamics of proteins as observed through Mößbauer spectra of ^{57}Fe. Fe is a constituent of heme groups and iron-sulfur redox centers in proteins, and hence, the observation of the dynamics of this atom is of obvious interest. Mößbauer spectra result from a resonant scattering of γ quants involving a suitable metastable state of the Mößbauer atom. The spectrum entails information about the motion of the atom during the lifetime of the metastable state. In the case of ^{57}Fe the spectrum is sensitive to the atomic motion in the time window 1ns - 100ns[6].

The observable, the spectral line shape function $I(\omega)$, is given by the expression[7]

$$I(\omega) \sim \text{Re } \hat{J}(i\omega) \qquad (11a)$$

where

$$\hat{J}(i\omega) = \int dx \, \exp(i\kappa x)[i\omega - L(x)]^{-1} \exp(-i\kappa x) \, p_o(x) \quad . \qquad (11b)$$

In this expression $\kappa = 7.3 \, \text{Å}^{-1}$ is the momentum of the γ quantum, $p_o(x)$ the Boltzmann distribution of ^{57}Fe in a potential $U(x)$ and $L(x)$ as given in Eq.(2c) with $k(x) = \Gamma/2$ where $\Gamma = 7 \cdot 10^6 \text{s}^{-1}$ is the natural linewidth of the metastable state. Obviously the shape of the Mößbauer spectrum is related to a correlation function of the type (4).

4. Approximation

The starting point for an evaluation of the observables discussed in Section 3 are Eqs.(4) and (6). These expressions are expanded for low and high frequencies

$$\hat{J}(\omega) \underset{\omega \to 0}{\sim} \sum_{n=0}^{\infty} \mu_{-(n+1)} (-\omega)^n \tag{12a}$$

$$\hat{J}(\omega) \underset{\omega \to \infty}{\sim} - \sum_{n=0}^{\infty} \mu_n \left(-\frac{1}{\omega}\right)^{n+1} \tag{12b}$$

The expansion coefficients are in the case of (4)

$$\mu_n = (-1)^n \int dx \; w(x) \{L^n(x)\}_b \, v(x) \tag{13a}$$

and in the case of (6)

$$\mu_n = (-1)^n \int dx \; v(x) \{[L^+(x)]^n\}_{b^+} \, w(x) \tag{13b}$$

These coefficients, the so-called generalized moments, can be constructed recursively in the order μ_0, μ_1, μ_2, ... and μ_{-1}, μ_{-2}, ... The determination of the moments with positive index is trivial. The coefficients with negative indices can be expressed by simple quadratures or evaluated numerically. For this purpose we consider the function $f_{-1}(x) = \{[L^+(x)]^{-1}\}_{b^+} w(x)$ which is defined equivalently by

$$L^+(x) \; f_{-1}(x) = w(x) \tag{14}$$

complemented with the boundary conditions specified by $\{ \quad \}_{b^+}$. If an algorithm to obtain $f_{-1}(x)$ for arbitrary $w(x)$ exists, one can evaluate μ_{-1} in (6) and also recursively μ_{-2}, μ_{-3} ... .

The latter require the intermediate solution of

$$L^+(x) \; f_{-2}(x) = f_{-1}(x) \quad , \text{ etc.,} \tag{14'}$$

(complemented again with the proper boundary conditions) which is equivalent to (14).

The solution of Eq.(14) can be expressed by a quadrature in the case that L^+ is given by (5) with $k(x) \equiv 0$. The solution depends on the boundary condition. In case $x_1 < x_2$ and $\kappa_1 = 0$, $\kappa_2 \to \infty$ which corresponds to example 1 of Section 3, the solution is

$$f_{-1}(x) = - \int_x^{x_2} dy \; [D(y) p_0(y)]^{-1} \int_{x_1}^y dz \; p_0(z) w(z) \quad . \tag{15}$$

Solutions for other boundary conditions and for moments expressed by (13a) can be constructed by means of the identities

$$L^+(x) = \exp[\beta U(x)] \; \partial_x \; \exp[-\beta U(x)] D(x) \; \partial_x \tag{16a}$$

$$L(x) = \partial_x \; \exp[-\beta U(x)] D(x) \; \partial_x \; \exp[\beta U(x)] \quad . \tag{16b}$$

The reader may also consult Gardiner[3] who solves this problem in the framework of the mean first passage time approximation.

In the case $k(x) \neq 0$ one can solve (14) by employing a discretization scheme for the Fokker-Planck operator which results in a tridiagonal matrix for L or L^+. For the inverse of a tridiagonal matrix one can apply the well-known Gaussian elimination procedure[8] and thereby determine $f_{-1}(x)$. The computational effort of the Gaussian elimination grows only linearly with the matrix dimension and, therefore, can be applied to dimensions of a few thousand. Below a certain mesh size the moments have been found to be independent of the discretization scheme. Hence, the moments can be constructed to include any desired features of the model potential surfaces.

We will now construct an approximate observable $\bar{j}(\omega)$ which reproduces the N_ℓ leading terms of the low-frequency expansion (12a) and the N_h leading terms of the high-frequency expansion (12b) where $N_\ell + N_h = 2N$ is even. The functional form of $\bar{j}(\omega)$ should be such that the corresponding time-dependent function $j(t)$ entails a series of exponentials. This implies that $j(\omega)$ can be expressed by the $(N+1,N)$ Padé approximants, i.e., fractions of polynomials in ω of degree $N+1$ (denominator) and N (numerator). Such Padé approximants have been constructed before[9] for one-sided conditions only, namely to reproduce the leading terms of the high-frequency expansion in ω^{-1}. However, so-called 2-sided Padé approximants can be constructed[10] which reproduce a desired behavior in ω and ω^{-1}. We have derived a representation best suited for numerical applications which reproduces the desired terms of both (12a) and (12b). The approximant, later on referred to as (N_h, N_ℓ), is

$$\hat{j}(\omega) = \sum_{n=0}^{N-1} (\underline{b}^n \underline{A} \underline{b}^n)^{-1} (\hat{\underline{a}} \cdot \underline{b}^n)(\underline{b}^n \cdot \underline{a})[\omega + \lambda_n]^{-1} \tag{17}$$

where

$$(\underline{a}^j)_i = \mu_{-N_\ell + i + j} \qquad i = 0, \dots, N-1; \; j = 0, \dots, N$$

$$\underline{a} = \hat{\underline{a}} = \underline{a}^{N_\ell/2} \qquad\qquad (N_\ell \text{ even})$$

$$\underline{a} = \underline{a}^{(N_\ell - 1)/2}; \; \hat{\underline{a}} = \underline{a}^{(N_\ell + 1)/2} \qquad (N_\ell \text{ odd})$$

$$\underline{A} = (\underline{a}^0, \dots, \underline{a}^{N-1}) \qquad\qquad (N \times N \text{ matrix})$$

(18)

and where λ_n and b_n are the eigenvalues and eigenvectors, respectively, of the Frobenius matrix

$$\underline{F} = \begin{bmatrix} 0 & 0 & 0 & \cdots & \gamma_0 \\ 1 & 0 & 0 & \cdots & \gamma_1 \\ 0 & 1 & 0 & \cdots & \gamma_2 \\ \vdots & & & & \vdots \\ 0 & \cdots & & 1 & \gamma_{N-1} \end{bmatrix} \tag{19}$$

Here, the vector γ is the solution of

$$\underline{A}\,\underline{\gamma} = \underline{a} . \tag{20}$$

The eigenvectors may be obtained recursively by means of

$$(\underline{b}^n)_0 = \gamma_0/\lambda_n; \quad (\underline{b}^n)_i = [(\underline{b}^n)_{i-1} + \gamma_i]/\lambda_n . \tag{21}$$
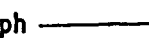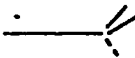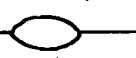
An equivalent representation of $\hat{j}(\omega)$ is furnished by expressing the $(N+1,N)$ Padé approximant in terms of a partial fraction expansion

$$\hat{j}(\omega) = \sum_{n=0}^{N-1} f_n/(\omega + \alpha_n) . \tag{22a}$$

The amplitudes f_n and relaxation constants α_n must obey

$$\sum_{n=0}^{N-1} f_n \alpha_n^m = \mu_m , \qquad m = -N_\ell, -N_\ell + 1, \dots, N_h - 1 . \tag{22b}$$

The algebraic solution of (22) is only feasible for N = 1,2. For larger N one should solve for f_n and α_n from Eqs.(17)-(21).

The algorithm presented is closely related to the well-known moment expansion of correlation functions[11] which reproduces systematically only the high-frequency dependence (12b). The approximant is commonly provided in terms of a continued fraction expansion which, however, is equivalent to a representation by means of the Padé approximant given here. The low-frequency dependence is accounted for by a "memory kernel" for which no systematic representation exists. In our description the "memory kernel" is disposed of in favor of 2-sided conditions enforcing the correct low-frequency behavior (12a). The reason why this route had not been tried before is connected with the need for the moments μ_{-1}, μ_{-2}, ... It had probably not been realized that algorithms for these moments do exist at least for problems which are essentially one-dimensional, e.g.,three-dimensional transport with spherical symmetry. We have succeeded in generalizing the construction of the moments μ_{-1}, μ_{-2}, ... also to situations which deviate from a one-dimensional linear structure of $L(x)$. Representing a tridiagonal L by a linear graph ———, the generalization applies also to nontridiagonal L corresponding to graphs with a finite number of structures ——— and ——⟨⟩—— and reactions at the graph end points. The moments μ_{-1}, μ_{-2}, ... are related to mean first passage times as shown in the following section. One can therefore expect that the current work on mean first passage times for higher dimensional problems will contribute also to the evaluation of μ_n's for a wider class of problems.

5. Relationship to the 'Mean First Passage Time' Approximation

The mean first passage time $\tau(x_0)$ describes the mean time which particles, starting at some position $x=x_0$, need to pass the position $x=x_2$ for the first time. It is assumed that the particles are described by Eqs.(2a)-(2c). Particles which arrive at $x=x_2$ are taken out to achieve measurement of <u>first</u> passage. This corresponds to the boundary condition (2d) with $\kappa_2 \to \infty$, i.e.,(8). The second spatial boundary condition at $x=x_1$ is dictated by particle number conservation and requires $\kappa_1=0$ in (2d). However, there are also more general boundary conditions possible. The mean first passage time $\tau(x_0)$ is accessible through the particle number correlation function

$$N(t|x_0) = \int dx\, p(x,t|x_0) \tag{23}$$

by means of the exponential approximation

$$N(t|x_0) = N_0 \exp[-t/\tau(x_0)]. \tag{24}$$

This approximation implies the identity

$$N_0\tau(x_0) = \int_0^\infty dt\, N(t|x_0). \tag{25}$$

In order to determine $\tau(x_0)$ one starts from the adjoint equation to (2a)

$$\partial_t p(x,t|x_0) = L^+(x_0)p(x,t|x_0). \tag{26}$$

Equations (23), (25) and the appropriate boundary conditions yield

$$L^+(x_0)\,\tau(x_0) = -1 \tag{27}$$

$$\partial_x \tau(x) = 0 \quad \text{at} \quad x=x_1 \; ; \quad \tau(x_2) = 0 .$$

This is the well-known differential equation for the mean first passage time[3,4].

In order to derive the relationship to the approximation in Section 4 we apply the algorithm derived to an observable with $v(x)=\delta(x-x_0)$, $w(x)\equiv 1$ and $N_\ell=1$, $N_h=1$. The leading terms of the low-frequency and high-frequency expansion are

$$\hat{N}(\omega|x_0) \sim N_0 \int dx \, \delta(x-x_0) \{(L^+)^{-1}\}_{b+}(-1) = \mu_{-1}(x_0) \tag{28a}$$

and

$$\hat{N}(\omega|x_0) \sim N_0 \int dx \, \delta(x-x_0)(1/\omega)\cdot 1 = N_0/\omega = \mu_0/\omega \tag{28b}$$

where we have introduced the above definition of the moments μ_0, μ_{-1}. If we now set $f(x)=N_0\{(L^+)^{-1}\}_{b+}(-1)$ or rather

$$L^+(x)\, f(x) = -N_0$$

applying the adjoint boundary conditions, a comparison with (27) shows $f(x)=\tau(x)N_0$. It follows $\mu_0=N_0$ and $\mu_{-1}=\tau(x_0)N_0$. If one now applies the algorithm of Section 4 one obtains according to Eq.(22b) $f_0\alpha_0^0=\mu_0$, $f_0\alpha_0^{-1}=\mu_{-1}$ and, hence, $f_0=\mu_0=N_0$, $\alpha_0^{-1}=\tau(x_0)$. Altogether, the algorithm yields

$$\hat{N}(\omega|x_0) \approx N_0/[\omega+\tau^{-1}(x_0)]$$

or rather Eq.(24).

In Ref. 12 the mean first passage time monoexponential approximation had been generalized to a biexponential approximation reproducing correctly μ_1, μ_0, μ_{-1} and μ_{-2} of a particle number correlation function. In this article we have generalized the theory to arbitrary correlation functions and to an arbitrary number of exponential contributions.

6. Results
    Figure 1 represents the observable of the first example of Section 3, the rate $\dot{N}(t)$ of absorbance of a particle diffusing freely from x_1 to x_2. The figure compares the exact rate with the approximants (N_h,N_ℓ) reproducing the N_h (N_ℓ) leading terms of the high (low)-frequency expansion. In this example the moments μ_{-1}, μ_{-2}, ... which correspond to $\hat{N}(0)$, $\ddot{N}(0)$, ... all vanish. The rate exhibits a typical threshold behaviour, i.e., the rate is completely flat and vanishes at short times and assumes nonzero values rather suddenly at later times. Such behavior is difficult to reproduce by a series of exponentials $\exp(\alpha_n t)$ and leads to spurious oscillations.
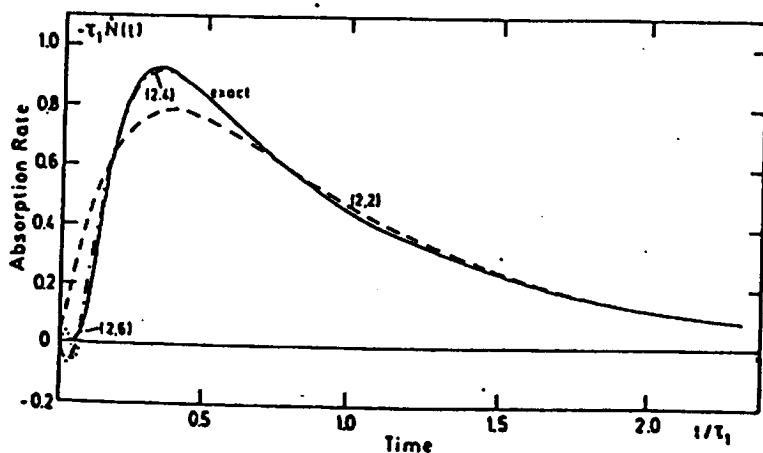
Fig. 1: Comparision of exact and approximate absorption rates for a particle diffusing linearly from x_1 to x_2 $[\tau_1 = (x_2 - x_1)^2/2D]$

Figure 1 shows that the most simple nontrivial approximation (2,2) which entails two exponential contributions describes rather correctly the overall increase, the maximum and the decay of the rate. Including more exponentials by way of (2,4) and (2,6) approximants leads to an improvement of the short-time behavior, albeit at the cost of the aforementioned spurious oscillations. The oscillations are connected with complex eigenvalues of the Frobenius matrix (19). In this respect this seemingly simple example actually constitutes a particularly difficult case, for in many other applications one can prove that oscillatory contributions do not arise.

The second example in Section 3 is concerned with the decay of fluorescence intensity as observed in a fluorescence microphotolysis experiment[5]. Figure 2 presents the fluorescence signal as observed in an actual experiment. The figure also demonstrates that the observed signal is described well by the evaluated fluorescence decay, proving thereby the validity of the theoretical description. The matching of the observed and calculated fluorescence signal yields the diffusion coefficient of the dye-labelled membrane constituents involved in the system investigated. In order to analyze the observations routinely a fast numerical procedure for the theoretical signal is desirable. The algorithm of Section 4 provides such procedure.
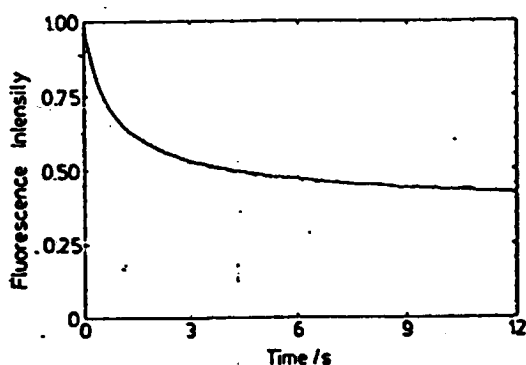

Fig. 2: Decay of the fluorescence intensity as observed in a Continuous Fluorescence Microphotolysis experiment and as calculated numerically (for details see Ref. 5)

Figure 3 compares the exact observable with the (8,0) and (0,8) approximants. The latter approximant yields by far the better description proving that the low-frequency expansion (12a) accounts for most of the fluorescence decay. Figure 3 also shows that a (2,6) approximant reproduces the fluorescence signal essentially exactly.

The third example considers the Mößbauer spectrum $I(\omega)$ of ^{57}Fe in proteins[13,14]. The accuracy of the observed spectrum is significant only in the central, low-frequency part of $I(\omega)$ and covers a time window of 1ns to 100ns. On this time scale the motion of a single atom in a protein is actually part of a concerted motion involving a larger protein fragment and, therefore, a large effective mass. One can safely describe this motion by the Fokker-Planck equation (2). In order to demonstrate the value of the algorithm developed here we consider the model of an ^{57}Fe atom diffusing in a harmonic potential.
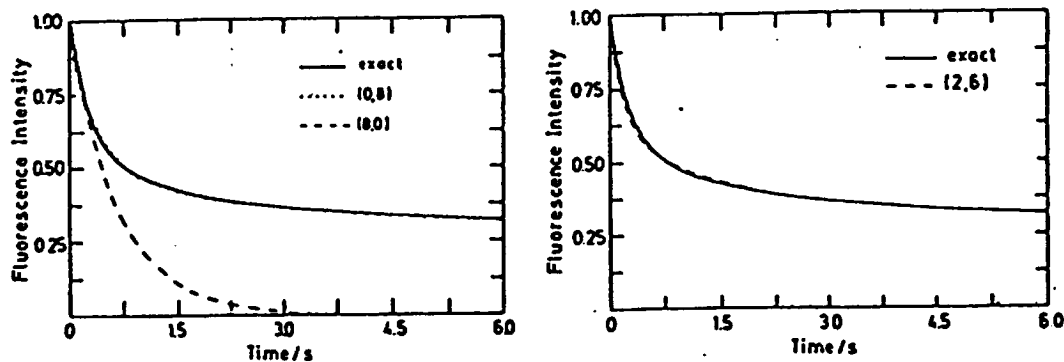

Fig. 3: Comparision of the exact and approximant fluorescence intensities

Figure 4 presents the exact spectrum obtained from the spectral expansion

$$J(\omega) = \exp(-a) \sum_{n=o}^{\infty} a^n / n! [i\omega + nD\kappa^2/a^2 + \Gamma/2] \qquad (29)$$

where $a = \kappa^2 \langle x^2 \rangle_T$, $\langle \rangle_T$ denoting the thermal average. This exact result is compared with various approximations, the moments reproduced in each case being indicated in Fig. 4. The comparision shows that the approximants reproducing 6 moments provide a satisfactory description of the Mößbauer spectrum. The central part of the spectrum, however, is described best if one chooses to reproduce the moments $\mu_{-5} - \mu_0$. The algorithm can be applied to essentially arbitrary potentials.

Studying a variety of potential shapes we have found that the observed Mößbauer spectra of proteins, in particular their temperature dependence, can be explained well with potentials exhibiting many minima. These minima correspond to metastable conformations of the proteins. The existence of such conformations had been previously suggested by Frauenfelder et al. The dynamics of proteins as monitored through Mößbauer spectra appears to originate from fluctuations between such metastable conformations.
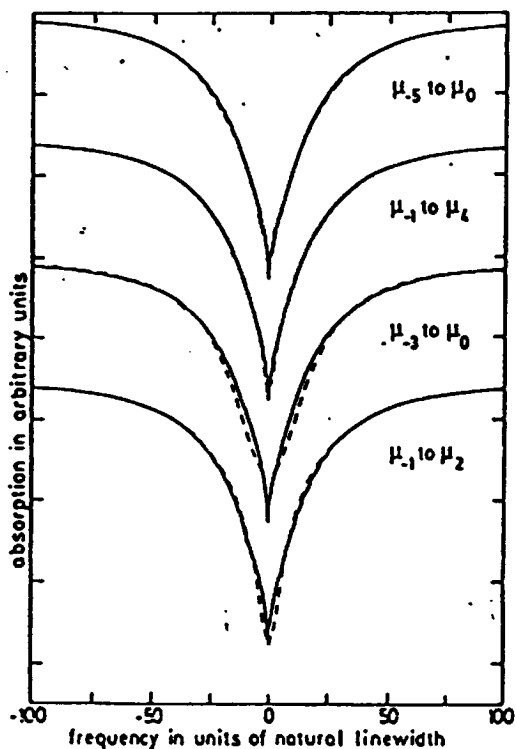
Fig. 4: Comparison of Mößbauer line shapes for Brownian motion in a harmonic oscillator ($D = 3 \cdot 10^6$ Å^2 s^{-1}, $\langle x^2 \rangle_T = 0.1$ Å^2) resulting from Eq.(29) (———) and from approximations reproducing the moments as indicated (----)

Acknowledgements

References

1. H. Frauenfelder, G.A. Petsko, and D. Tsernoglu, Nature 280, 558-563 (1979).

2. N.G. van Kampen, "Stochastic Processes in Physics and Chemistry", (North Holland Publ. Comp., Amsterdam, 1981).

3. C.W. Gardiner, "Handbook of Stochastic Methods" (Springer, Berlin, 1983).

4. A. Szabo, K. Schulten, and Z. Schulten, J. Chem. Phys. 72, 4350-4357 (1980).

5. R. Peters, A. Brünger and K. Schulten, Proc. Natl. Acad. Sci. USA **78**, 962-966 (1981).

6. See for example F. Parak, E.N. Frolov, R.L. Mößbauer and V.I. Goldanskii, J. Mol. Biol. **145**, 825-833 (1981).

7. This can be readily derived from Eq.(5) in K.S. Singwi and A. Sjölander, Phys. Rev. **120**, 1093 (1960).

8. See for example B. Noble, "Applied Linear Algebra" (Prentice Hall, Englewood Cliffs, N.J., 1969).

9. O. Goscinski and E. Brändas, Int. J. Quant. Chem. **5**, 131-156 (1971).

10. W.B. Jons, W.J. Thron and H. Waadeland, Trans. Am. Math. Soc., **261**, 503-529 (1980); A. Ag. Németh and Gy. Paris, J. Math. Phys. **22**, 1192-1195 (1981).

11. See for example S. Grossmann, Phys. Rev. A. **17**, 1123-1132 (1978) and references therein.

12. K. Schulten, Z. Schulten and A. Szabo, J. Chem. Phys. **74**, 4426-4432 (1981).

13. W. Nadler and K. Schulten, Phys. Rev. Lett. **51**, 1712-1715 (1983).

14. W. Nadler and K. Schulten (to be submitted).